Electronic Supplementary Material (ESI) for Materials Horizons.

Supporting Information

Tailoring double-layer aromatic polymer with multi-active sites towards high performance aqueous Zn-organic batteries

Yi Zhao,[a] Yongxin Huang,*[a,b,c] Renjie Chen,*[a,b,c] Feng Wu,[a,b,c] and Li Li*[a,b,c,d]

[a] Beijing Key Laboratory of Environmental Science and Engineering, School of Materials Science and Engineering, Beijing Institute of Technology, Beijing, 100081, China
[b] Advanced Technology Research Institute, Beijing Institute of Technology, Jinan, 250300, China
[c] Collaborative Innovation Center of Electric Vehicles in Beijing, Beijing, 100081, China
[d] Guangdong Key Laboratory of Battery Safety, Guangzhou Institute of Energy Testing, Guangdong, 511447, China

Experimental Procedures

Electropolymerization of C@poly(AP): The three C@poly(AP) cathodes were prepared by a typical electrochemical polymerization process according to our previous report.[1] All the chemicals were purchased from Aladdin Co., China without further purification. At first, the nanoporous carbon slurry was made by mixing nanoporous carbon power (C, Beike 2D materials Co., Ltd.), acetylene black, and poly(vinylidene fluoride) (PVDF) into N-methyl pyrrolidone (NMP) at a weight ratio of 8:1:1. Second, the obtained nanoporous carbon slurry was pasted onto a rectangular carbon cloth (WOS1009, CeTech. Co.), followed by drying overnight at 100 °C. Third, the carbon-coated carbon fabric was used as work electrode in a three-electrode system containing 1 M H2SO4 and 0.03 M monomers of 2-AP, 3-AP or 4-AP. With using an Ag/AgCl (saturated potassium chloride) as reference electrode and a Pt mesh as counter electrode, the electrochemical polymerization was conducted by running linear cyclic voltammetry (CV) test at 20 mV s^{-1} and within the voltage range from –0.3 to 1.1 V for 30 cycles. Finally, the obtained C@poly(AP) substrate was removed out from the H_2SO_4 electrolyte and rinsed repeatedly with using distilled water and then dried at 60 °C for 6 hours. Similarly, we also collected the poly(AP) precipitation after the electropolymerization for Raman, Fourier transform infrared spectroscopy (FTIR) and X-ray photoelectron microscopy (XPS) measurements to prove the successful growth of polymers onto nanoporous carbon.

Fabrication double-layer C@poly(3-AP)/poly(4-AP) cathode: The dual-layer of C@poly(3-AP)/poly(4-AP) cathode was fabricated by a novel two-step electrochemical polymerization process of in-situ electrodepositing poly(3-AP) and poly(4-AP) onto nanoporous carbon in sequence. Typically, the C@poly(3-AP) was firstly prepared by running the CV polymerization for 2, 5, 10 cycles, respectively, into a three-electrode system containing 0.03 M 3-AP monomer, similarly to the electropolymerization of C@poly(AP). Subsequently, the obtained C@poly(3-AP) was cleaned by distilled water and immediately dipped into another three-electrode system containing 0.03 M 4-AP molecules followed by CV polymerization at 20 mV s^{-1} for 20 cycles. The purpose of the different polymerization CV cycles was to control the mass ratio of poly(3-AP) and poly(4-AP). Finally, the obtained heterogeneous dual-layer organic samples, named as C@poly(3-AP)/poly(4-AP)-2, C@poly(3-AP)/poly(4-AP)-5 and C@poly(3-AP)/poly(4-AP)-10, respectively, were rinsed repeatedly by distilled water, then dried at 60 °C for 6 hours. The nanoporous carbon slurry was repeatly pasted onto carbon fabric to electrodeposite more polymers, and obtain the high mass loading of C@poly(3-AP)/poly(4-AP) cathodes (2 to 30 mg cm^{-2}) .

Electrochemical characterization and DFT calculations: CR2032-type button cells were prepared by stacking C@poly(AP) and C@poly(3-AP)/poly(4-AP) sample as cathode, respectively, a glass fiber membrane soaked with 2 M $ZnSO_4$ solution as separator, and the high-purity 80 µm-thick Zn foil as anode together. Note that the Zn foil can provide an areal capacity more than 30 mAh cm^{-2} in theory, which is to avoid the effect of Zn anode fading. The CV was performed on a CS 350H electrochemical workstation (Wuhan Corr Test Instruments Co., Ltd). The galvanostatic charge–discharge (GCD) was carried out with a Land Battery Test System. The area loading of composite for each electrode is from 2.0 to 32 mg cm^{-2}, except that for in situ FTIR test is about 10 mg cm^{-2}. The structural optimization and energy levels determination of three organic molecules and their polymers were calculated by the all-electron density functional program DMol3 of Materials Studio 2019.[2,3] The Generalized Gradient Approximation–Becke Lee Yang Parr (GGA-BLYP) functional and the double numerical plus polarization (DNP) basis set were used. The binding energies between organic molecules and Zn^{2+} ions were performed using the CASTEP code based on the density functional theory (DFT) principle. The kinetic energy cutoff for the plane wave expansion was set to 350 eV. The convergence tolerance for the maximum force was set 0.01 eV Å^{-1}.

Supporting Figures, Discussions and Tables

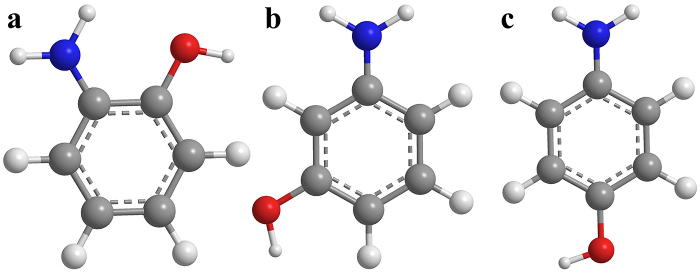

Fig. S1 3D geometries of the aminophenol monomer (a) 2-AP, (b) 3-AP and (c) 4-AP at relaxation, respectively.

The theoretical capacity for polymers (C_{theory}, mAh g^{-1}) is calculated using the following equations:

$C_{theory}=(n_e*F)/(M*3.6)$..(1)

Where the ne is the electron value of one unit of polymers reacted with Zn^{2+}. F is the faraday constant, and 1 F= 96485 C mol^{-1}, and M (g mol^{-1}) represents the molar mass of the polymer unit.

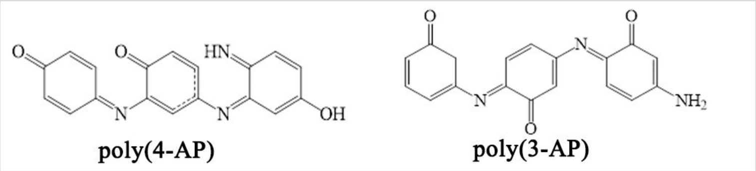

$M_{poly(4\text{-}AP)}$=18C*12+3O*16+3N*14+12H*1 =318 g mol^{-1}...(2)

$M_{poly(3\text{-}AP)}$=18C*12+3O*16+3N*14+12H*1 =320 g mol^{-1}...(3)

Hence,

$C_{poly(4\text{-}AP)}$=(5*96485)/(318*3.6)=421 mAh g^{-1} ....(4)

$C_{poly(3\text{-}AP)}$=(5*96485)/(320*3.6)=418 mAh g^{-1} ....(5)

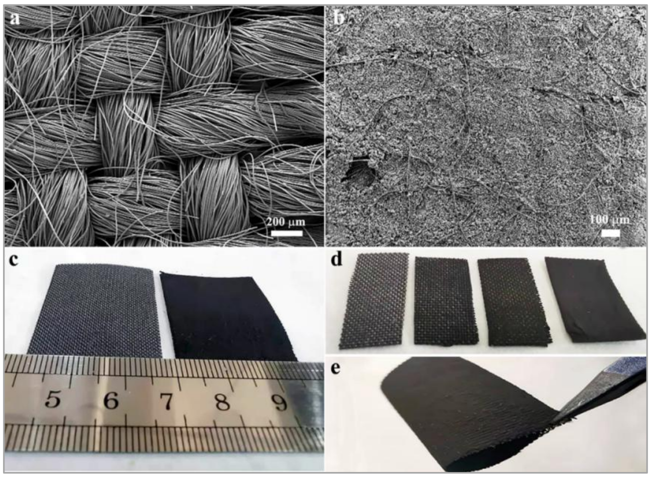

Fig. S2 (a and b) SEM images of a carbon cloth used as the current collector and nanoporous-carbon-coated carbon cloth, respectively. (c) Photograph showing the large size of two carbon fabrics with and without coated nanoporous-carbon, respectively. (d) Photograph showing the four carbon fabrics with and without electrodeposited polymers, the order from left to right is bare carbon cloth, carbon-coated carbon cloth, C@poly(4-AP), C@poly(3-AP)/poly(4-AP). (e) The large size of flexible C@poly(3-AP)/poly(4-AP) as cathode with the mass loading of 6.0 mg cm^{-2}.

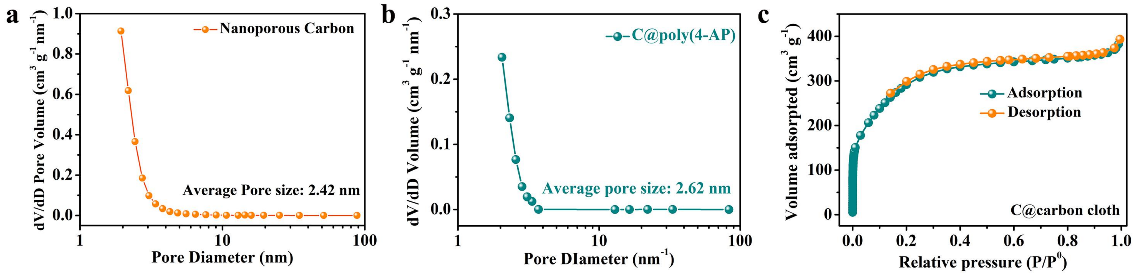

Fig. S3 Pore size distributions of (a) nanoporous carbon and (b) C@poly(4-AP) coating, respectively. (c) N_2 adsorption/desorption isotherms of nanoporous carbon coating.

After the nanoporous carbon coating on the carbon cloth, the specific surface area is decreased to 861 m^2 g^{-1}, which is due to the addictive of carbon black and PVDF binder (Fig. S3c). After polymerization, the specific area and average pore size of C@poly(4-AP) are changed to 492 m^2 g^{-1} and 2.63 nm, respectively (Fig. 1h and S3b). Hence, the poly(4-AP) nanodots electrodeposited on nanoporous carbon, as shown in Fig. 1d,e, is not only existed in the surface of nanoporous carbon, but also filled into its nanopores, which is benefit to the stability and conductivity of the polymers.

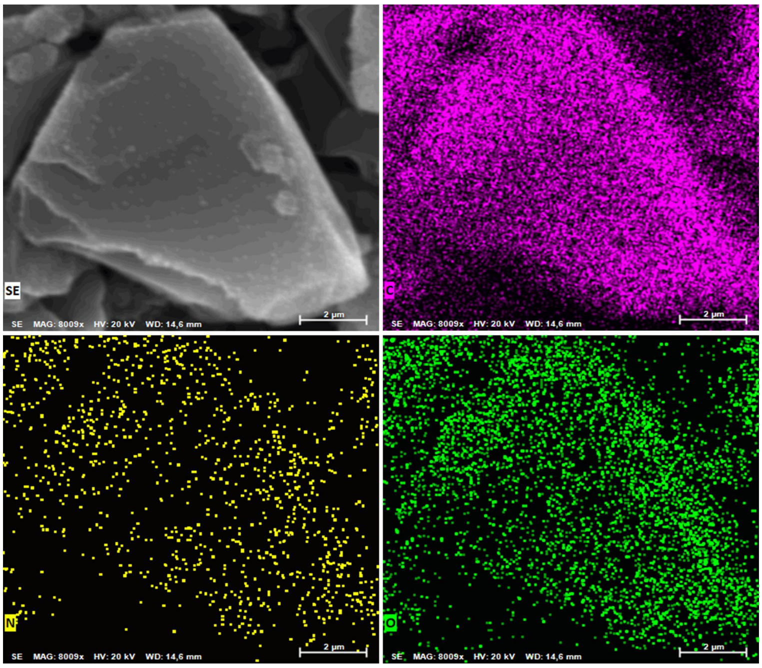

Fig. S4 STEM-EDS mapping of C, N, and O distributions in C@poly(4-AP) cathode.

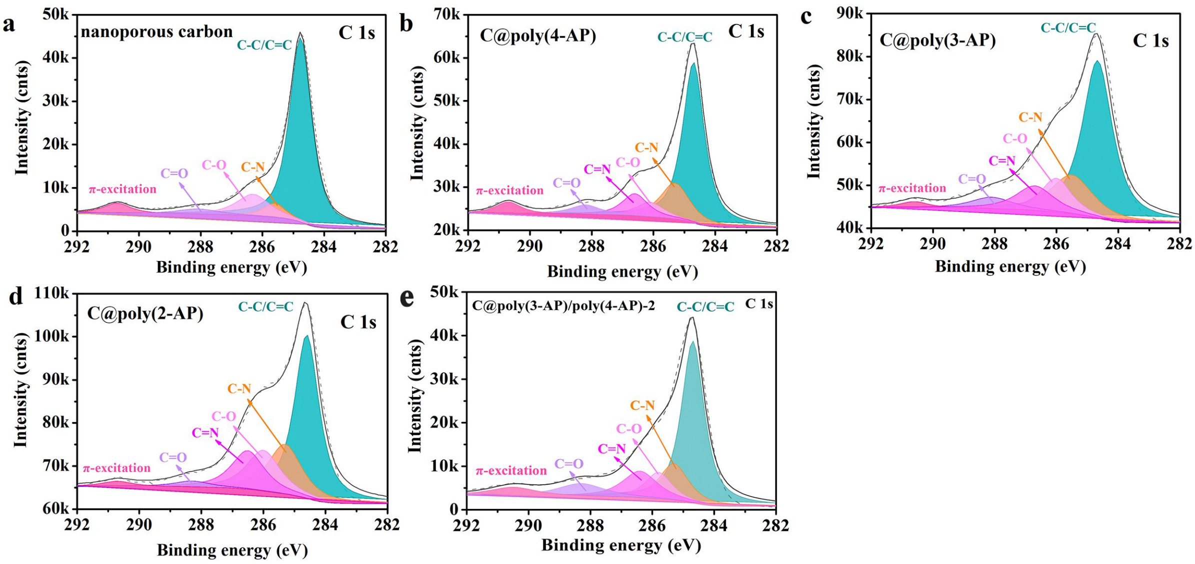

Fig. S5 High-resolution XPS spectral profiles of C 1s of (a) nanoporous carbon, (b) C@poly(4-AP), (c) C@poly(3-AP), (d) C@poly(2-AP) cathodes, and (e) C@poly(3-AP)/poly(4-AP)-2 cathodes respectively.

Compared to nanoporous carbon and C@poly(4-AP), the increased percentage of C=O and C=N peaks prove the successfully synthesis of the double-layer C@poly(3-AP)/poly(4-AP) composite.

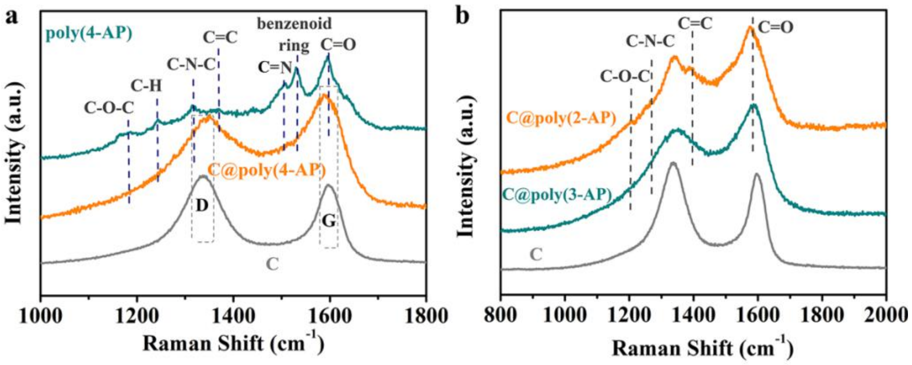

Fig. S6 (a) Raman spectrum of nanoporous carbon (C), pure poly(4-AP) and C@poly(4-AP) cathodes, respectively. (b) Raman spectrum of nanoporous carbon (C), C@poly(3-AP) and C@poly(2-AP) cathodes, respectively.

Compared with the nanoporous carbon sample, the broader D and G peaks of C@poly(4-AP) cathode are induced by the electrodeposited poly(4-AP) nanodot arrays. Besides, the ascribed C-N-C and C-O-C peaks confirm an effective synthesis of C@poly(AP) organic materials.

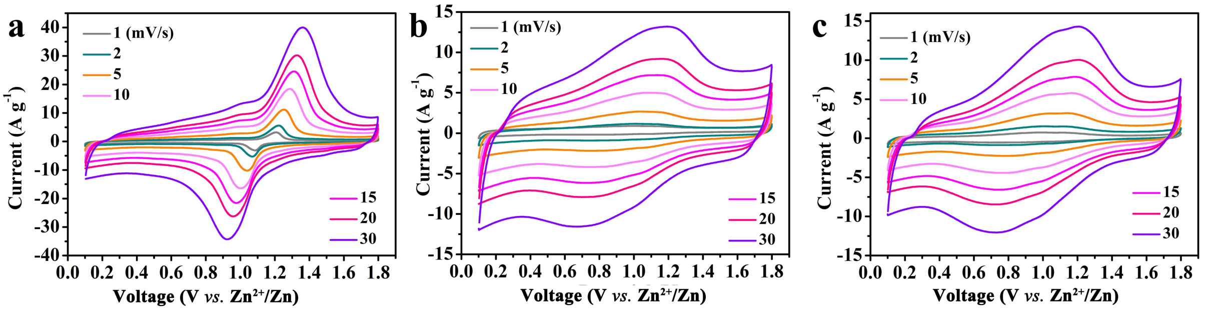

Fig. S7 (a) CV curves of typical C@poly(2-AP)//Zn, (b) C@poly(3-AP)//Zn, and C@poly(4-AP)//Zn cells, respectively.

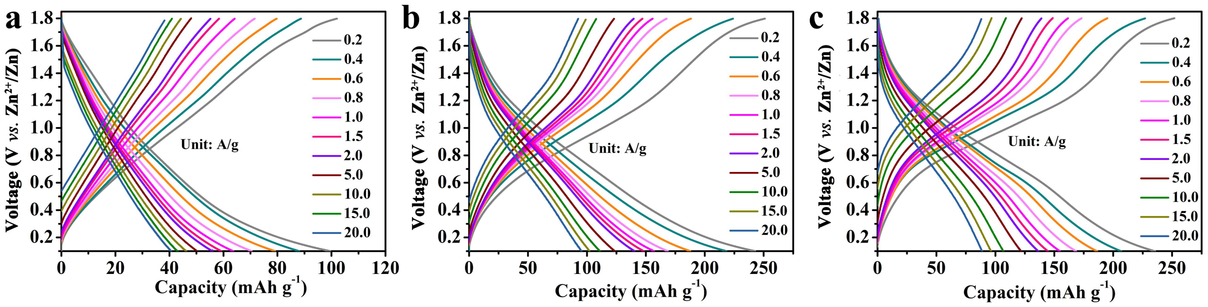

Fig. S8 CD curves of typical (a) nanoporous carbon//Zn, (b) C@poly(3-AP)//Zn and (c) C@poly(2-AP)//Zn cells, respectively.

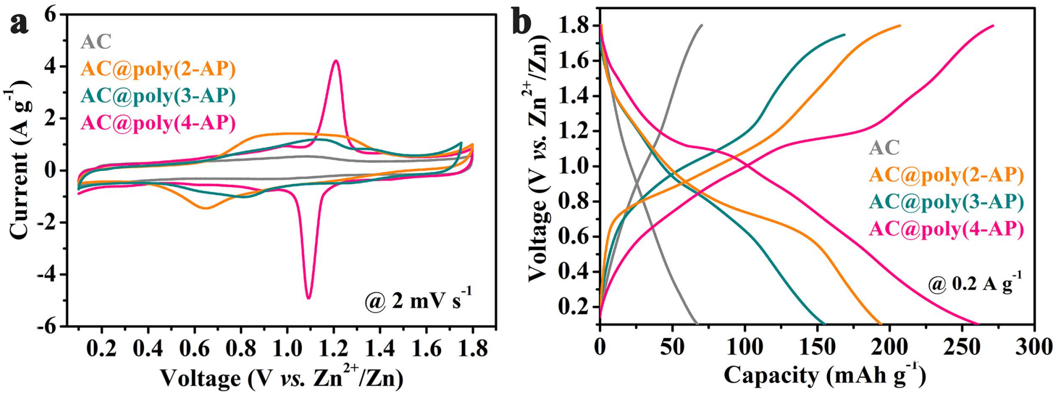

Fig. S9 (a) CV and (b) CD curves of typical active carbon(AC)//Zn, AC@poly(3-AP)//Zn and C@poly(2-AP)//Zn cells, respectively.

In our previous work, we have proved that the polymer can not only filled into the nanopores, but also coated onto the outer surfaces of carbon-based materials.[1] Therefore, nanoporous carbon not only benefits to the growth of polymers, but also helps to obtain high mass loading organic cathodes, which is adequate for practical application of Zn-organic batteries. Compared with nanoporous carbon with 3174 m^2 g^{-1}, the active carbon (AC, YP80) with the specific area of 2280 m^2 g^{-1} has been used to electrodeposite the three polymers. To better understand the effective of carbon-based materials, Zn//AC@poly(AP) cells were assembled to study the energy storage performances. The inferior capacities of AC@poly(AP) cathodes further confirm the important role of nanoporous carbon with ultrahigh specific area, as displayed in Fig. S9.

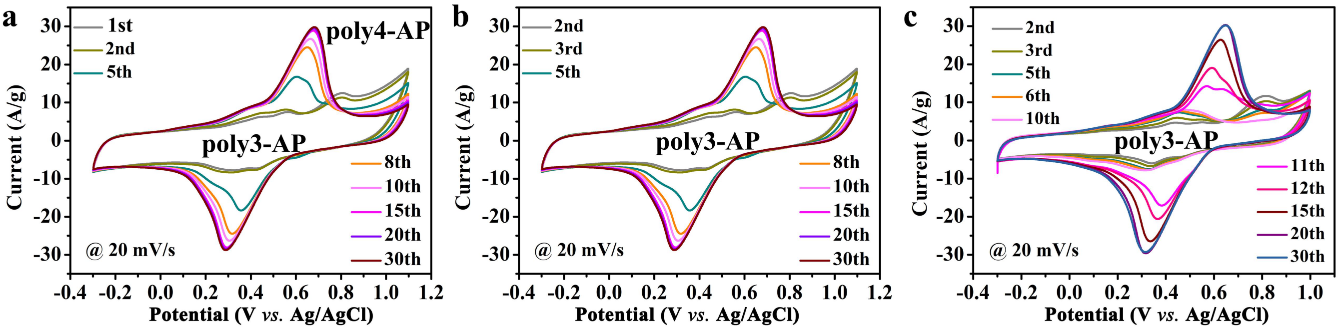

Fig. S10 The evolution of CV loops during the process of electrodepositing poly(3-AP) and poly(4-AP) onto nanoporous carbon, obtaining the composite cathodes of a) C@poly(3-AP)/poly(4-AP)-2, b) C@poly(3-AP)/poly(4-AP)-5, and c) C@poly(3-AP)/poly(4-AP)-10.

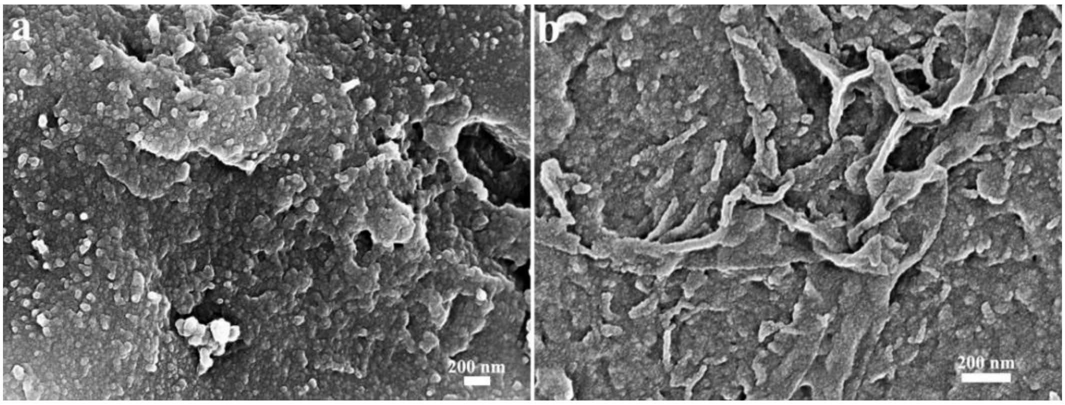

Fig. S11 SEM images of the electrodeposited (a) poly(3-AP) and (b) poly(3-AP)/poly(4-AP)-2 over nanoporous carbon, respectively.

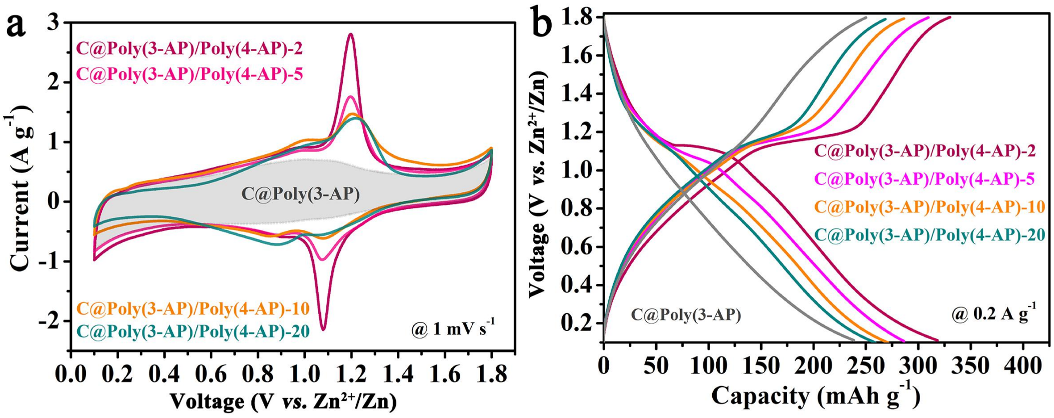

Fig. S12 (a, b) CV and CD curves of ZIBs with the cathodes of C@poly(3-AP) and C@poly(3-AP)/poly(4-AP) with different mass ratio of poly(3-AP) and poly(4-AP), respectively.

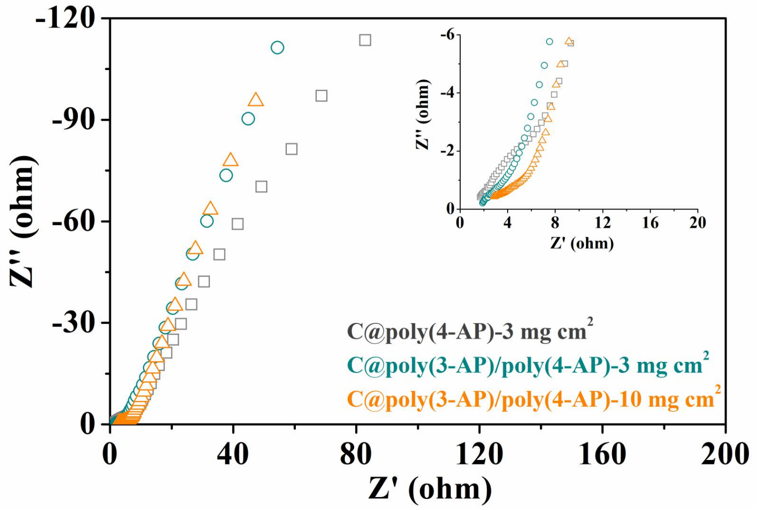

Fig. S13 EIS spectra of Zn//C@poly(4-AP) and Zn//C@poly(3-AP)/poly(4-AP), respectively.

To better understand the superior rate capability of C@poly(4-AP) and C@poly(3-AP)/poly(4-AP) cathodes, EIS spectra have been exhibited in Fig. S12. The total ohmic resistance of Zn//C@poly(4-AP) and Zn//C@poly(3-AP)/poly(4-AP) are both less than 2 Ω, reflecting the fast migration of Zn^{2+} in the aqueous electrolyte. Furthermore, the charge transfer resistance (Rct) of the two Zn-organic cells are no more than 10 Ω in the middle frequency, indicating the fast zinc-ion kinetic and superior rate performance of the organic/organic cathode. Moreover, C@poly(3-AP)/poly(4-AP) cathode at the 10 mg cm^{-2} still has the small total ohmic resistance and Rct, reflecting the good conductivity of carbon-based polymers even at high mass loading. We have added and highlighted this discussion in the supporting information.

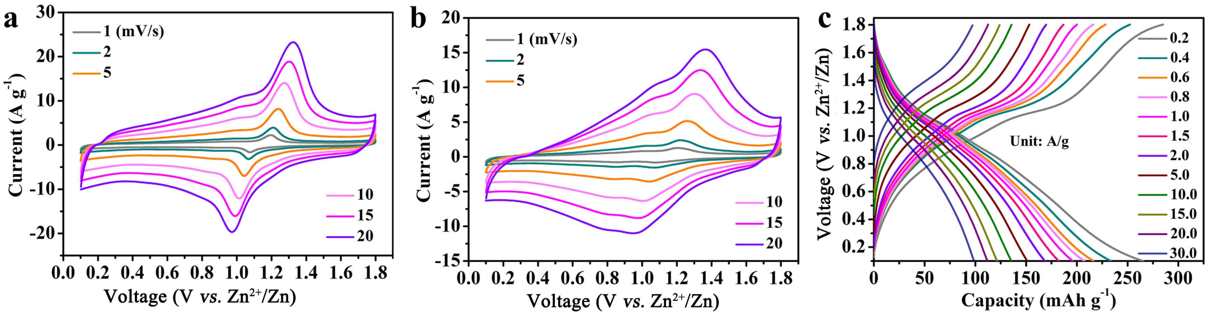

Fig. S14. (a) CV curves of the C@poly(3-AP)/poly(4-AP)-2 cathode. (b) CV and (c) CD curves of the C@poly(3-AP)/poly(4-AP)-10 cathode, respectively.

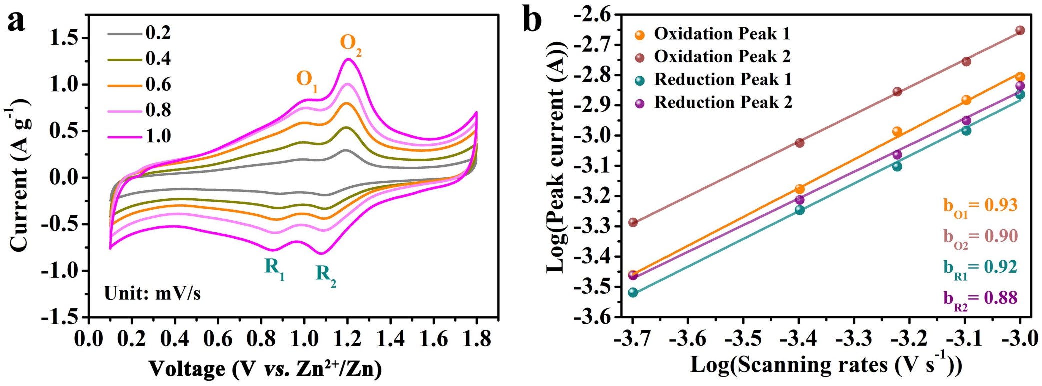

Fig. S15 (a) CV curves of a typical Zn-C@poly(3-AP)/poly(4-AP)-10 cell, according to which the b-values for Oxidation (O_1 and O_2) and Reduction (R_1 and R2) peaks are deduced, as shown in (b).

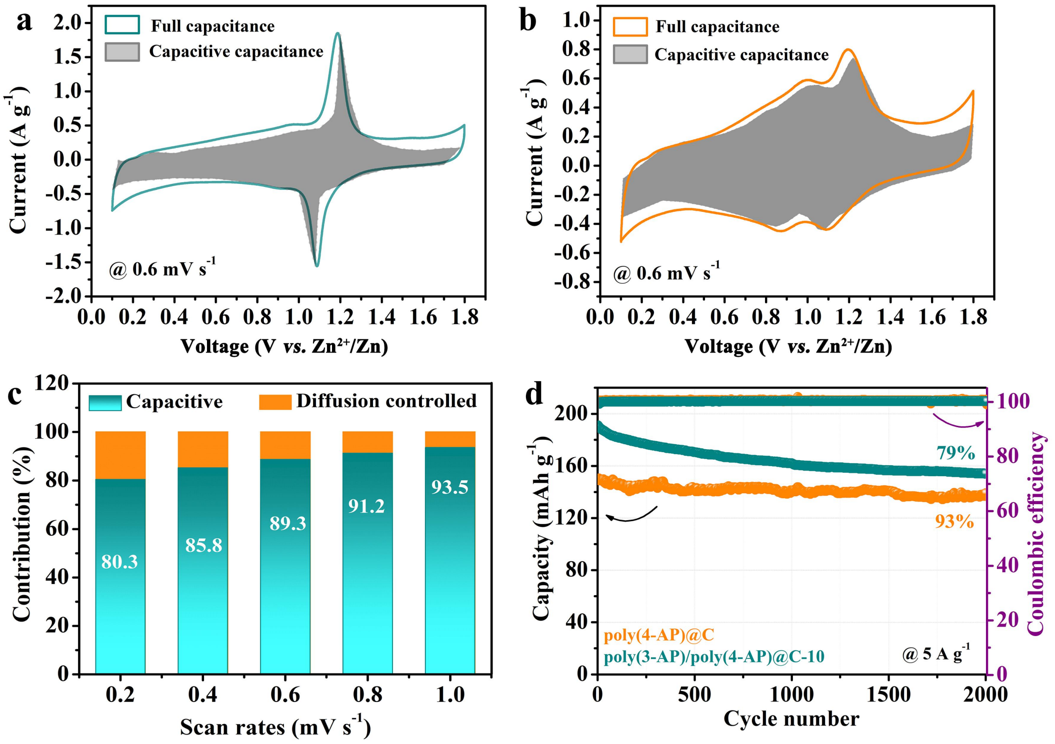

Fig. S16 (a) CV curves of C@poly(3-AP)/poly(4-AP)-2 and (b) C@poly(3-AP)/poly(4-AP)-10 with the capacitive-like fraction at a scan rate of 0.6 mV s^{-1}, respectively. (c) Capacitive contribution ratios at corresponding scan rates of the C@poly(3-AP)/poly(4-AP)-10 cathode. (d) Cycling stability of the C@poly(3-AP)/poly(4-AP)-2 cathode tested at 5 A g^{-1} over 2000 cycles.

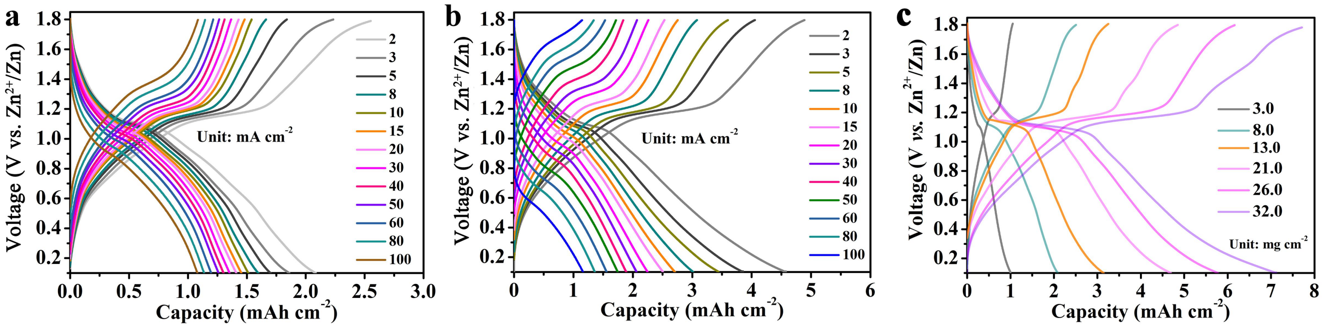

Fig. S17 CD profiles at different current densities of C@poly(3-AP)/poly(4-AP)-2 with the mass loading of (a) 8 mg cm^{-2}, (b) 21 mg cm^{-2}, respectively. (c) CD profiles of C@poly(3-AP)/poly(4-AP)-2 at 1 mA cm^{-2} with different mass loading of active materials.

As revealed, the carbon based organic-organic composite shows slow capacity degradation with the mass loading from 2.9 to 32 mg cm^{-2}, even more than 69% capacity retention and superior rate performance at the practical mass loading.

Fig. S18 Two Zn//C@poly(3-AP)/poly(4-AP)-2 cells with the mass loading of 21 mg cm^{-2} were connected in series to derive the purple LEDs.

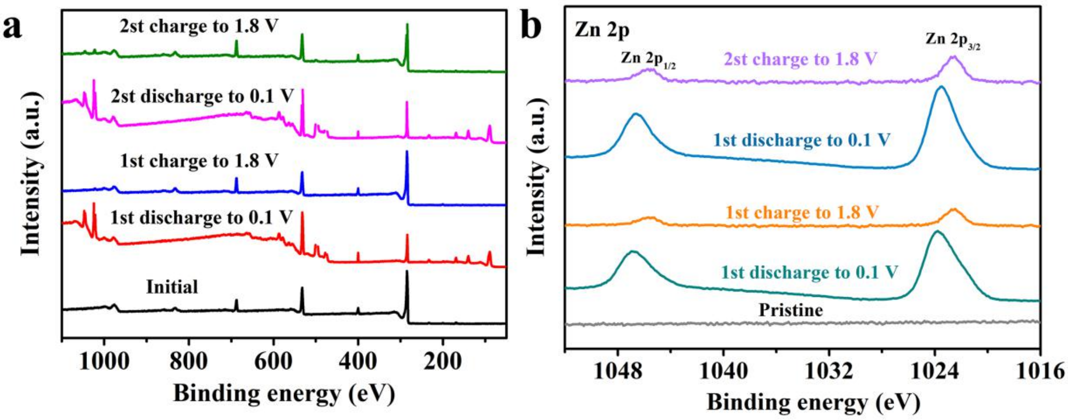

Fig. S19 (a) and (b) are survey XPS spectra and high-resolution Zn 2p spectra of C@poly(3-AP)/poly(4-AP) in the first two cycles, respectively.

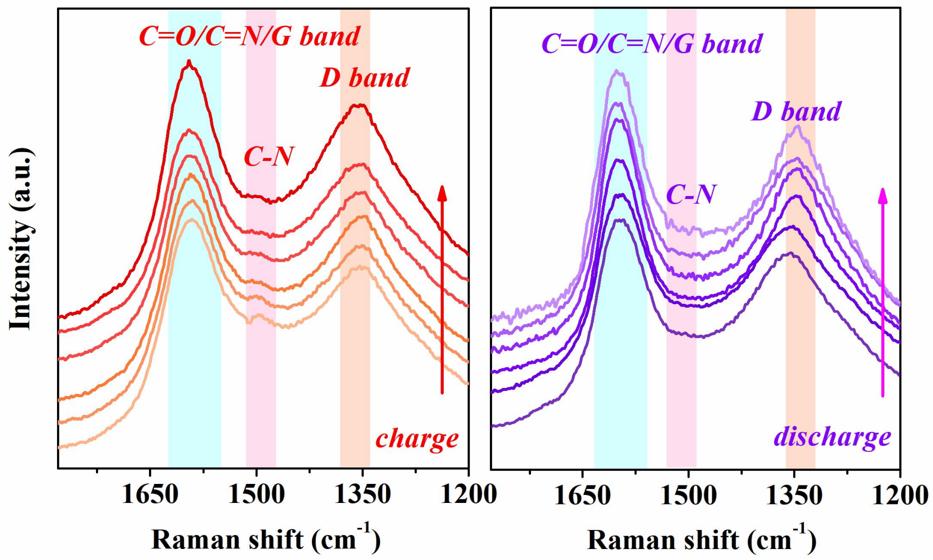

Fig. S20 In situ Raman characterizations of Zn-C@poly(3-AP)/poly(4-AP) batteries during charging and discharging process.

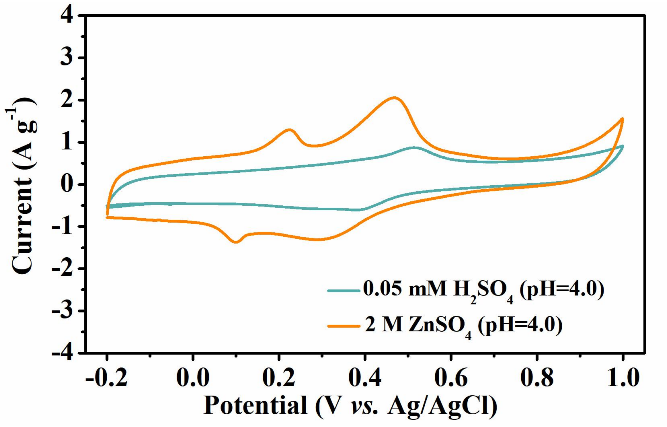

Fig. S21 CV curves at 2 mV s^{-1} of the C@poly(3-AP)/poly(4-AP) electrode in different electrolytes tested in a three electrode system.

As exhibited in Fig. S19, the dissolution of $Zn_4(OH)_6SO_4{\cdot}5H_2O$ flakes in the organic/organic cathode is contributed by the released H+ from the polymer cathodes during the first few charging cycles, which has been proved by the previous reported work.[1] To further support the co-insertion/removal of H^+/Zn^{2+}, the CV curves of the C@poly(3-AP)/poly(4-AP) electrode in a three electrode system with 0.05 mM H_2SO_4 (pH=4.0) and 2 M $ZnSO_4$ (pH=4.0) electrolyte, separately, were tested (Fig. S21).[20] The CV curve in 0.05 mM H_2SO_4 electrolyte is contained in the CV curve in 2 M $ZnSO_4$ electrolyte, demonstrating the insertion of H+ in 2 M ZnSO4 electrolyte. The redox peaks at 0.1 V/0.22 V and 0.45 V/0.35 V are corresponding to the redox reactions of poly(3-AP) and poly(4-AP) with Zn^{2+}/H^+, respectively. Moreover, the C@poly(3-AP)/poly(4-AP) cathode exhibit the larger area and redox peak currents in Zn||2 M $ZnSO_4$||C@poly(3-AP)/poly(4-AP) cell than that in three electrode system using Pt as ounter electrode, as displayed in Fig. 4a, proving the capacity contributed by the insertion of Zn^{2+} acts as the leading role in the organic/organic hybrid cathodes. Thus, the binding energy of the polymers inserted with Zn^{2+} was preferred to calculate using DFT calculation.

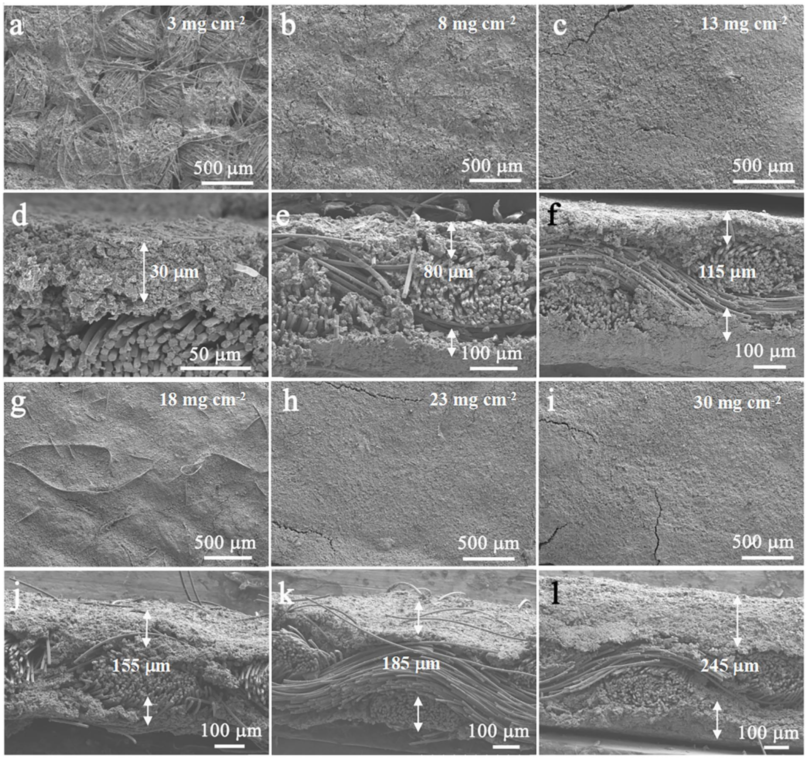

Fig. S22 Top-view and cross-sectional SEM imagines of C@poly(3-AP)/poly(4-AP)-2 with different mass loading, respectively.

Fig. S2a shows the SEM image of the carbon fiber fabric used as the current collector. Fig. S2c shows the optical photograph of the carbon fabric coated with nanoporous carbon. After the electrodeposition of poly(3-AP) and poly(4-AP), a photograph of this cathode is shown in Fig. S2d,e. The mass loading of nanoporous carbon coating over a carbon cloth can be adjusted by controlling the coating times of blade-coating. For a thinner C@poly(3-AP)/poly(4-AP)-2 electrode (3 mg cm^{-2}), a large number of carbon fibers could be exposed, as shown in Figs. S22a. With increasing the mass loading of C@poly(3-AP)/poly(4-AP)-2, the organic/organic electrode has a more smooth surface. Moreover, the thickness of the C@poly(3-AP)/poly(4-AP)-2 increases from ~30 μm to 245 μm as shown in Fig. S22 d-f, j-l, which was further compressed in the Zn-organic cell. The loose structure of the carbon fabric and nanoporous carbon are benefit for the fast kinetics and rate capability of the organic/organic hybrid cathodes with high mass loading.

Table S1 Binding energies between Zn^{2+} ions and various chemical bonds in molecules.

Binding energy	2-AP	3-AP	4-AP	3-AP & 4-AP
$E_{O\text{-}Zn\text{-}O}$ (eV)	-2.936	-3.872	-3.532	-3.962 eV
$E_{O\text{-}Zn\text{-}O}$ (eV)	-4.204	-3.456	-2.958	-3.536 eV
$E_{N\text{-}Zn\text{-}O}$ (eV)	-3.015	-3.796	-3.225	-3.429 eV (3N4O) -3.625 eV (3O4N)

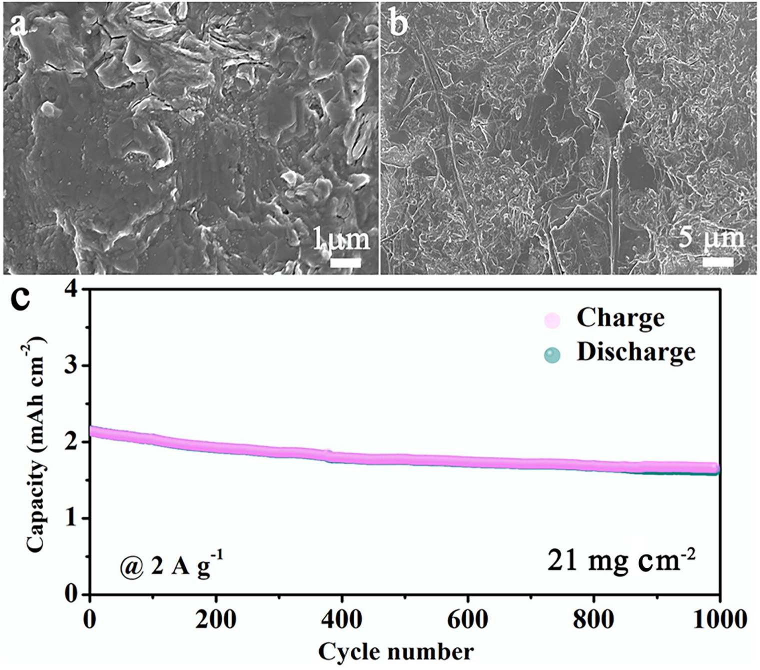

Fig. S23 (a) Low- and high-resolution SEM imagines of Zn anode after 1000 cycles at 2A g^{-1}, respectively. (c) The cycling performance of Zn//C@poly(3-AP)/poly(4-AP)-2 after 1000 cycles.

Fig. S23c displayed the cycling performance of Zn//C@poly(3-AP)/poly(4-AP)-2 cell with the mass loading. Hence, C@poly(3-AP)/poly(4-AP)-2 exhibits good cycling stability (85% capacity retention after 1000 cycles) under both high mass loading and low current density 2 A g^{-1}. The rough surface of the Zn anode can be responsible for the capacity decay after long cycling tests, as shown in Fig. S23a,b.

Table S2 Electrochemical performance comparison of reported organic cathode materials for aqueous rechargeable zinc batteries, corresponding to Fig. 4h.

Organic cathode	**Structure**	**Mass loading** mg cm^{-2}	**Electrolyte**	**Discharge average voltage & Voltage range**	**Reversible capacity @ current rate**	**Cycling performance**	**Reference**
PANI	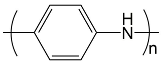	1.5	1 M Zn(CF$_3$SO$_3$)$_2$	1.0V 0.5–1.5 V	200 mAh g^{-1}@50 mA g^{-1} 95 mAh g^{-1}@5000 mA g^{-1}	82 mAh g^{-1}@5000 mA g^{-1} 92%@the 3000th cycle	4
PANI	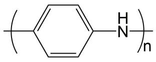	0.6	1 M ZnSO$_4$	1.0V 0.5–1.6 V	184 mAh g^{-1}@200 mA g^{-1} 130 mAh g^{-1}@10000 mA g^{-1}	110 mAh g^{-1}@10000 mA g^{-1} 85%@the 3000th cycle	5
C4Q	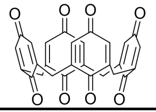	2.5 ~10	3 M Zn(CF$_3$SO$_3$)$_2$	1.0 V 0.2–1.8 V	335 mAh g^{-1}@20 mA g^{-1} 140 mAh g^{-1}@500 mA g^{-1}	122 mAh g^{-1}@500 mA g^{-1} 87%@the 1000th cycle	6
PTO	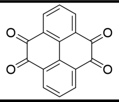	4.0~6.0	2 M ZnSO$_4$	0.8 V 0.36–1.46 V	336 mAh g^{-1}@40 mA g^{-1} 110 mAh g^{-1}@20000 mA g^{-1}	207 mAh g^{-1}@3000 mA g^{-1} 70%@the 1000th cycle	7
Chloranil	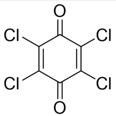	3.0~5.0	1 M Zn(CF$_3$SO$_3$)$_2$	1.1 V 0.8–1.4 V	205 mAh g^{-1}@43 mA g^{-1}	118 mAh g^{-1}@217 mA g^{-1} 70%@the 200th cycle	8

DTT	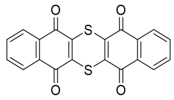	5.0	2 M $ZnSO_4$	0.76 V 0.3–1.4 V	211 mAh g^{-1}@50 mA g^{-1} 100 mAh g^{-1}@200 mA g^{-1}	100 mAh g^{-1}@2000 mA g^{-1} 84%@the 23000th cycle	9
TCNAQ	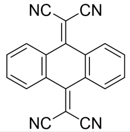	5~ 10	2 M $ZnSO_4$	1.1 V 0.6–1.8 V	169 mAh g^{-1}@50 mA g^{-1} 55 mAh g^{-1}@50 mA g^{-1}	117 mAh g^{-1}@500 mA g^{-1} 81%@the 1000th cycle	10
PBQS	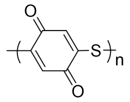	1.0	3 M $Zn(CF_3SO_3)_2$	0.95 V 0.2–1.8 V	203 mAh g^{-1}@20 mA g^{-1} 125 mAh g^{-1}@100 mA g^{-1}	175 mAh g^{-1}@40 mA g^{-1} 86%@the 50th cycle	11
HqTp	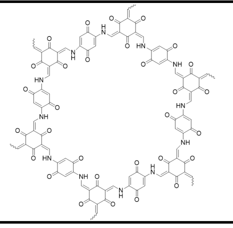	1.0	3 M $ZnSO_4$	0.87 V 0.2–1.8 V	276 mAh g^{-1}@125 mA g^{-1} 125 mAh g^{-1}@1250 mA g^{-1}	85 mAh g^{-1}@3750 mA g^{-1} 95%@the 1000th cycle	12
PDB	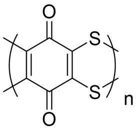	1.0~5.0	4 M $Zn(CF_3SO_3)_2$	0.93 V 0.2–1.55 V	234 mAh g^{-1}@20 mA g^{-1} 176 mAh g^{-1}@10000 mA g^{-1}	170 mAh g^{-1}@20000 mA g^{-1} 75%@the 10000th cycle	13
PDBS	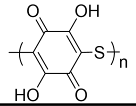	1.0~1.5	2 M $ZnSO_4$	0.6 V 0.3–1.45 V	260 mAh g^{-1}@10 mA g^{-1} 160 mAh g^{-1}@5000 mA g^{-1}	245 mAh g^{-1}@1000 mA g^{-1} 94%@the 1000th cycle	14
Poly(1,5-NAPD)	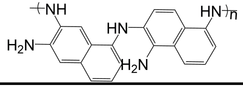	2.5~30.0	2 M $ZnSO_4$	0.8 V 0.1–1.8 V	307 mAh g^{-1}@200 mA g^{-1} 145 mAh g^{-1}@14800 mA g^{-1}	150 mAh g^{-1}@10000 mA g^{-1} 91%@the 10000th cycle	1
PQ-Δ	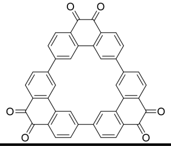	2.0	3 M $Zn(CF_3SO_3)_2$	0.78 V 0.25–1.6 V	203 mAh g^{-1}@30 mA g^{-1}	210 mAh g^{-1}@150 mA g^{-1} 99.9%@the 500th cycle	15
HATN	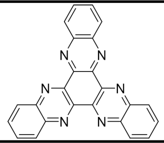	1.5	2 M $ZnSO_4$	0.53 V 0.3–1.1 V	370 mAh g^{-1}@100 mA g^{-1} 123 mAh g^{-1}@20000 mA g^{-1}	150 mAh g^{-1}@5000 mA g^{-1} 93%@the 5000th cycle	16
PTCDA	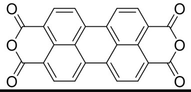	2.5~12.3	2 M $ZnCl_2$	0.5 V 0.05–1.0 V	123 mAh g^{-1}@200 mA g^{-1} 78 mAh g^{-1}@32000 mA g^{-1}	100 mAh g^{-1}@8000 mA g^{-1} 81%@the 500th cycle	17
PC/G	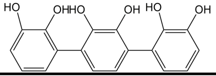	2.0	3 M $ZnSO_4$	0.8 V 0.2–1.9 V	355 mAh g^{-1}@50 mA g^{-1} 171 mAh g^{-1}@5000 mA g^{-1}	230 mAh g^{-1}@1000 mA g^{-1} 64%@the 2000th cycle	18
HATN-3CN	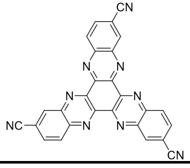	1.0	2 M $ZnSO_4$	0.64 V 0.1–1.6 V	320 mAh g^{-1}@50 mA g^{-1} 190 mAh g^{-1}@20000 mA g^{-1}	266 mAh g^{-1}@5000 mA g^{-1} 91%@the 5800th cycle	19
TAPQ	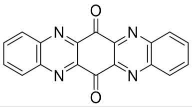	3.0~4.0	1 M $ZnSO_4$	0.84 V 0.5–1.6 V	270 mAh g^{-1}@50 mA g^{-1} 80 mAh g^{-1}@5000 mA g^{-1}	270 mAh g^{-1}@50 mA g^{-1} 94%@the 260th cycle	20
PANI at low temperature	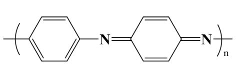	17.3	7.5 M $ZnCl_2$	0.91 V 0.5-1.5 V	100 mAh g^{-1}@50 mA g^{-1} 40 mAh g^{-1}@1000 mA g^{-1}	85 mAh g^{-1}@200 mA g^{-1} ~99%@the 2000th cycle	21

P(4VC86-stat-SS14)	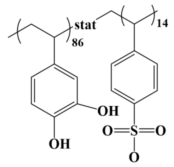	2.5	4 M $Zn(TFSI)_2$	1.1 V 0.5-1.7 V	324 mAh g^{-1}@340 mA g^{-1} 196 mAh g^{-1}@204000 mA g^{-1}	184 mAh g^{-1}@10200 mA g^{-1} ~83%@the 48000th cycle	22
m-PTPA	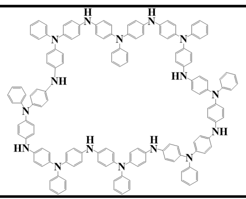	1.8-2.2	2 M $ZnCl_2$	1.15 V 0.6-1.7 V	210 mAh g^{-1}@340 mA g^{-1} 107 mAh g^{-1}@6000 mA g^{-1}	104 mAh g^{-1}@6000 mA g^{-1} ~87.6%@the 1000th cycle	23
HAQ-COF	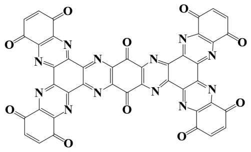	4.0-6.0	2 M $ZnSO_4$	0.85 V 0.3-1.6 V	344 mAh g^{-1}@100 mA g^{-1} 96 mAh g^{-1}@10000 mA g^{-1}	150 mAh g^{-1}@5000 mA g^{-1} 75%@the 10000th cycle	24
P(4VC$_{86}$-stat-SS$_{14}$)	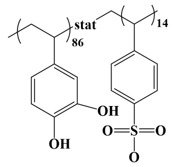	0.5-30.0	4 M $Zn(TFS_2)$	1.12 V 0.55-1.65 V	325 mAh g^{-1}@344 mA g^{-1} 96 mAh g^{-1}@150000 mA g^{-1}	100 mAh g^{-1}@3340 mA g^{-1} 75%@the 400th cycle	25
C@poly(4-AP)	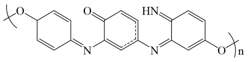	2.5	2 M $ZnSO_4$	1.05 V 0.1–1.8 V	308 mAh g^{-1}@200 mA g^{-1} 156 mAh g^{-1}@20000 mA g^{-1}	195 mAh g^{-1}@5000 mA g^{-1} 79%@the 2000th cycle	**This Work**
C@poly(3-AP)/poly(4-AP)	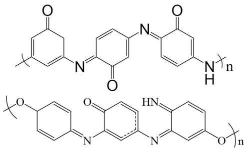	**2.5~32.0**	2 M $ZnSO_4$	**1.0 V** **0.1–1.8 V**	**350mAh g^{-1}@200 mA g^{-1}** **167 mAh g^{-1}@30000 mA g^{-1}**	**195 mAh g^{-1}@5000 mA g^{-1}** **91%@the 2000th cycle**	**This Work**

Table S3 N/P ratios and utilization of the anode for different mass loading of the active materials in our organic/organic hybrid electrodes.

Mass loading (mg cm^{-2})	3	8	13	21	26	32
$r_{N/P}$	46.5	21.5	14.8	10.0	8.1	6.6
CE (%)	96.2	95.4	94.8	94.1	93.5	91.3

The N/P ratio is a important parameter for the practical application of Zn-organic batteries. To better obtain the capacity of C@poly(AP) and C@poly(3-AP)/poly(4-AP) cathodes, the 80 μm-thick polished Zn foil with the areal capacity of 46.8 mAh cm^{-2} in theory was used as the anodes, which is much surplus to the organic cathode even at the 32 mg cm^{-2}. The N/P ratio can be calculated by the following equations:

$$r_{N/P}=C_{Zn}/C_{organic/organic}=46.8/C_{organic/organic}$$

Where the $C_{organic/organic}$ is about the areal capacity of the C@poly(3-AP)/poly(4-AP)-2 with different mass loading. The utilization of anode can be obtained form the coulombic efficiency (CE) of the CD curves, as displayed in Fig. S17c.

References

[1] Y. Zhao, Y. N. Wang, Z. M. Zhao, J. W. Zhao, T. Xin, N. Wang, J. Z. Liu, *Energy Storage Mater. 2020,* **28**, 64.

[2] Y. C. Fan, Y. Zhao, S. Li, Y. Lv, Y. Zhu, R. Xiang, S. Maruyama, H. Zhang, Q. F. Zhang. *J. Energ. Chem. 2021,* **59***,* 63.

[3] Y. Huang, Z. Wang, M. Guan, F. Wu, R. Chen, *Adv. Mater*. 2020*,* **32***,* 2003534.

[4] F. Wan, L. Zhang, X. Wang, S. Bi, Z. Niu, J. Chen, *Adv. Funct. Mater.* 2018*,* **28***,* 1804975

[5] H. Y. Shi, Y. J. Ye, K. Liu, Y. Song, X. Sun, *Angew. Chem. Int. Ed.* 2018*,* **57***,* 16359.

[6] Q. Zhao, W. Huang, Z. Luo, L. Liu, Y. Lu, Y. Li, L. Li, J. Hu, H. Ma*, J. Chen, Sci. Adv.* 2018, **4**, eaao1761.

[7] Z. Guo, Y. Ma, X. Dong, J. Huang, Y. Wang, Y. Xia, *Angew. Chem. Int. Ed.* 2018, **57**, 11737.

[8] D. Kundu, P. Oberholzer, C. Glaros, A. Bouzid, E. Tervoort, A. Pasquarello, M. Niederberger, *Chem. Mater.* 2018, **30**, 3874.

[9] Y. Wang, C. Wang, Z. Ni, Y. Gu, B. Wang, Z. Guo, Z. Wang, D. Bin, J. Ma, Y. Wang, *Adv. Mater.* 2020, **32**, 2000338.

[10] Q. Wang, X. Xu, G. Yang, Y. Liu, X. Yao, *Chem. Commun.* 2020*,* **56**, 11859.

[11] G. Dawut, Y. Lu, L. Miao, J. Chen, *Inorg. Chem. Front.* 2018, **5**, 1391-1396.

[12] A. Khayum, M. Ghosh, V. Vijayakumar, A. Halder, M. Nurhuda, S. Kumar, M. Addicoat, S. Kurungot, R. Banerjee, *Chem. Sci.* 2019*,* **10**, 8889.

[13] J. Xie, F. Yu, J. Zhao, W. Guo, H.-L. Zhang, G. Cui, Q. Zhang, *Energy Storage Mater. 2*020, **33**, 283.

[14] T. Sun, Z.-J. Li, Y.-F. Zhi, Y.-J. Huang, H. J. Fan, Q. Zhang, *Adv. Funct. Mater*. 2021, 2010049.

[15] K. W. Nam, H. Kim, Y. Beldjoudi, T.-w. Kwon, D. J. Kim, J. F. Stoddart, *J. Am. Chem. Soc.* 2020,**142**, 2541.

[16] Z. Tie, L. Liu, S. Deng, D. Zhao, Z. Niu, *Angew. Chem. Int. Ed.* 2020, **59**, 1.

[17] H. Zhang, Y. Fang, F. Yang, X. Liu, X. Lu, *Energy Environ. Sci.* 2020, **13**, 2515.

[18] S. Zhang, W. Zhao, H. Li, Q. Xu, *Chem.Sus Chem.* 2019, **13**, 188.

[19] Z. Ye, S. Xie, Z. Cao, L. Wang, D. Xu, H. Zhang, J. Matz, P. Dong, H. Fang, J. Shen, M. Ye, *Energy Storage Mater.* 2021, **37***,* 378.

[20] Y. J. Gao, G. F. Li, F. Wang, J. Chu, P. Yu, B. S. Wang, H. Zhan, Z. P. Song, *Energy Storage Mater.* 2021, ISSN 2405.

[21] Q. Zhang, Y. L. Ma, Y. Lu, L. Li, F. Wan, K. Zhang, J. Chen, *Nat. Commun.* 2020, **11**, 4463.

[22] N. Patil, C. Cruz, D. Ciurduc, A. Mavrandonakis, J. Palma, R. Marcilla, *Adv. Energy Mater.* 2021, **11**, 2100939.

[23] H. Z. Zhang, L. F. Zhong, J. H. Xie, F. Yang, X. Q. Liu, X. H. Lu, *Adv. Mater.* 2021, 33, 2101857.

[24] W. X. Wang, V. S. Kale, Z. Cao, Y. J. Lei, S. Kandambeth, G. D. Zou, Y. P. Zhu, E. Abouhamad, O. Shekhah, L. Cavallo, M. Eddaoudi, H. N. Alshareef, *Adv. Mater.* 2021, **2103617**.

[25] N. Patil, J. Palma, R. Marcilla, *Polymers* 2021, **13**, 1673.